Ecological Modelling 291 (2014) 15–27

Contents lists available at ScienceDirect

Ecological Modelling

journal homepage: www.elsevier.com/locate/ecolmodel

Assimilating remote sensing information into a coupled hydrology-crop growth model to estimate regional maize yield in arid regions

Yan Li [a], Qingguo Zhou [a], Jian Zhou [b,*], Gaofeng Zhang [a], Chong Chen [a], Jing Wang [c]

[a] School of Information Science and Engineering, Lanzhou University, Lanzhou 730000, China
[b] Cold and Arid Regions Environmental and Engineering Research Institute, Chinese Academy of Sciences, Lanzhou 730000, China
[c] Lanzhou Institute of Arid Meteorology, China Meteorological Administration, Key Laboratory of Arid Climatic Change and Reducing Disaster of Gansu Province, Key Open Laboratory of Arid Climate Change and Disaster Reduction of China Meteorological Administration, Lanzhou 730000, China

ARTICLE INFO

Article history:
Received 25 January 2014
Received in revised form 11 July 2014
Accepted 12 July 2014

Keywords:
EnKF
Coupled hydrology-crop growth model
Remote sensing information
EFAST

ABSTRACT

Regional crop yield prediction is a significant component of national food policy making and security assessments. A data assimilation method that combines crop growth models with remotely sensed data has been proven to be the most effective method for regional yield estimates. This paper describes an assimilation method that integrates a time series of leaf area index (LAI) retrieved from ETM+ data and a coupled hydrology-crop growth model which links a crop growth model World Food Study (WOFOST) and a hydrology model HYDRUS-1D for regional maize yield estimates using the ensemble Kalman filter (EnKF). The coupled hydrology-crop growth model was calibrated and validated using field data to ensure that the model accurately simulated associated state variables and maize growing processes. To identify the parameters that most affected model output, an extended Fourier amplitude sensitivity test (EFAST) was applied to the model before calibration. The calibration results indicated that the coupled hydrology-crop growth model accurately simulated maize growth processes for the local cultivation variety tested. The coefficient of variations (CVs) for LAI, total above-ground production (TAGP), dry weight of storage organs (WSO), and evapotranspiration (ET) were 13%, 6.9%, 11% and 20%, respectively. The calibrated growth model was then combined with the regional ETM+ LAI data using a sequential data assimilation algorithm (EnKF) to incorporate spatial heterogeneity in maize growth into the coupled hydrology-crop growth model. The theoretical LAI profile for the near future and the final yield were obtained through the EnKF algorithm for 50 sample plots. The CV of the regional yield estimates for these sample plots was 8.7%. Finally, the maize yield distribution for the Zhangye Oasis was obtained as a case study. In general, this research and associated model could be used to evaluate the impacts of irrigation, fertilizer and field management on crop yield at a regional scale.

1. Introduction

Crop growth and yield data are critical for informing national food security and agricultural operation and management. A range of factors, including increasingly augmented populations, reduced cropland acreage and water resources, environmental deterioration, and global climate change, significantly affect agricultural production and threaten food security. Therefore, accurate regional crop growth monitoring and yield prediction are vital for the sustainable development of agriculture. In the past decades, crop growth monitoring and crop yield predictions have moved away from conventional techniques, such as agro-meteorological model forecasting and the establishment of relationships between remote sensing spectral vegetation indexes and field measurements, in favour of more integrated approaches (e.g. Dente et al., 2008; de Wit et al., 2012; Fang et al., 2011; Liang and Qin, 2008; Ma et al., 2013; Xu et al., 2011). For instance, operational systems for regional crop monitoring and yield forecasting now usually rely on an integrated analysis of weather data, crop simulation model results and satellite observations.

Using the biophysical principles of plant growth, crop growth models can provide detailed estimates of crop states, including phenological status, leaf area index (LAI) and yield for specific crop types. The most commonly used crop growth model, WOFOST,

* *Corresponding author*. Tel.: +86 931 4967724.
E-mail addresses: liyan_2007@lzu.edu.cn (Y. Li), zhouqg@lzu.edu.cn (Q. Zhou), zhoujian@lzb.ac.cn (J. Zhou), zhanggaof@lzu.edu.cn (G. Zhang), chenchong87@gmail.com (C. Chen), wangjing1102@126.com (J. Wang).

http://dx.doi.org/10.1016/j.ecolmodel.2014.07.013
0304-3800/

has been applied to evaluations of production potential, optimized crop management, and yield gap quantification for various crops (Van Laar et al., 1997; Bouman et al., 2001; Wolf, 2002) in addition to studies of the effects of environmental variability and climatic change on crop production (Kropff et al., 1996; ten Berge et al., 1997; Tsuji et al., 1998; Matthews and Stephens, 2002). However, in WOFOST, the soil water balance is calculated using a "tipping bucket" approach within three compartments (i.e. a root zone, a transmission zone, and a groundwater zone) under water-limited conditions. This approach oversimplifies simulations of the hydrologic cycle in crop growth models (Eitzinger et al., 2004; Priesack et al., 2006). In reality, variation in available soil moisture is a main driver of variation in crop yield (Rodriguez-Iturbe et al., 2001; Shepherd et al., 2002; Anwar et al., 2003; Patil and Sheelavantar, 2004), and accurate estimates of soil moisture are critical for understanding crop status and yield. To enhance the ability of the WOFOST model to simulate the hydrologic cycle, model coupling is needed. Linkages between models have recently received attention from researchers. For example, Casanova and Judge (2008) coupled a land surface process (LSP) model with a widely used crop-growth model (DSSAT) to estimate energy and moisture fluxes in dynamic vegetation. Maruyama and Kuwagata (2010) linked land surface and crop growth models to estimate the effects of growing season changes on the energy balance and water use in rice paddies. Van den Hoof et al. (2011) coupled the Land Environment Simulator (JULES) and a crop-growth model (SUCROS) to evaluate the hydrological cycle and vegetation effects on energy, water, and carbon fluxes.

Crop models are very useful in evaluating crop growth and yield at the field scale, but their implementation at a regional scale is restricted by input data availability at the corresponding scale, which results in models that may not produce results with adequate accuracy for practical applications (Chipnashi et al., 1999; Moulin and Guerif, 1999; Mignolet et al., 2007). To overcome the difficulties inherent to these modelling approaches, the integration of remote sensing observations and crop growth models has been recognized as an important approach for monitoring crop growth conditions and estimating yield at a regional scale (Dente et al., 2008; de Wit et al., 2012; Fang et al., 2011; Liang and Qin, 2008; Ma et al., 2012; Xu et al., 2011). In recent years, extensive efforts have been made to integrate crop growth models with remote sensing information based on the "assimilation strategy" (Chen et al., 2012; Revill et al., 2013). Satellite data can provide a synoptic overview of actual growing conditions and can be used to diagnose discrepancies from normal conditions. For example, a Normalized Difference Vegetation Index (NDVI; Rouse and Haas, 1973) profile of the current year could be compared to the average historic profile for a given crop (Kogan, 1998; Liu and Kogan, 2002). Moreover, satellite data can be used to complement crop model simulation results by including, for example, the impacts of fire, frost, or drought during sensitive crop stages.

In general, the integration of remote sensing observations and crop growth models is often achieved through data assimilation. There are two basic strategies for data assimilation: (1) recalibration/re-initialization methods and (2) sequential assimilation algorithms, such as the EnKF. The recalibration/re-initialization approach commonly uses optimization algorithms to re-initialize or re-parameterize a crop growth model by adjusting initial conditions or input parameters to minimize the merit function between remotely sensed biophysical parameters and simulated parameters (Dente et al., 2008; Fang et al., 2011; Ma et al., 2013). However, this method cannot incorporate dynamic changes, such as state variable updates or dynamic crop growth simulations. For sequential assimilation algorithms, a primary assumption is that improvements in a state variable made in the previous step can enhance the estimation accuracy in the next step. Because this approach can combine many types of observations taken at discrete time steps, the state variables can be continually updated and more accurately simulated. In particular, the EnKF, which is a sequence filter algorithm that combines a probabilistic approach with sequential data assimilation, can account for sequential uncertainty in remotely sensed observations (Curnel et al., 2011; Dorigo et al., 2007; Quaife et al., 2008) and nonlinear structural characteristics in crop growth models (de Wit and Van Diepen, 2007; Vazifedoust et al., 2009). Several EnKF assimilation schemes with different degrees of complexity and integration have been developed and evaluated during the last decade (Curnel et al., 2011; de Wit and Van Diepen, 2007; Vazifedoust et al., 2009; Jin et al., 2010).

In this study, we present a novel method for estimating regional maize yield that assimilates LAI values derived from remote sensing imagery into a coupled hydrology-crop growth model (which links the WOFOST and HYDRUS models) using an EnKF. This method can ultimately be used to estimate crop yields at a regional scale.

2. Material and methods

2.1. Study area

We applied our coupled model to the agricultural system in the Zhangye Oasis (Fig. 1), an arid region in the middle reaches of the Heihe River basin, northwest China. This area has a typical temperate continental climate, with mean annual precipitation and potential evaporation ranging from 60 to 280 mm and 1000 to 2000 mm, respectively. This agricultural system, which primarily cultivates maize and wheat, employs a highly developed irrigation system that was constructed in the last few decades. The main water resource for irrigation in this area originates from the Heihe River and the groundwater.

2.2. Observation data

In 2008, the Watershed Allied Telemetry Experimental Research (WATER) program (Li et al., 2009), part of the Chinese Academy of Sciences' Action Plan for Western Development, was applied to this region to study the ecological and hydrological processes of agricultural systems (methodological information for this program can be found at http://westdc.westgis.ac.cn/data). The primary biophysical, biochemical, meteorological and hydrological parameters used in our study were obtained through this program, predominantly from the Yingke station (38°51′N, 100°25′ E, altitude 1519 m a.s.l.). Research at this agro-ecological station focused on eco-hydrological processes during maize growth periods and provided data (interval: 30 min) on regional meteorology, physical soil properties, and soil moisture dynamics. Meteorological data included net radiation, solar radiation, maximum air temperature, minimum air temperature, precipitation, wind speed, atmospheric pressure, and relative humidity.

The status of maize was intensively monitored throughout its entire growth period, which lasted from April 20, 2008 through September 22, 2008. The sowing date, emergence date and harvest date were April 20, May 6, and September 22, respectively. Data on LAI were measured once every 15 days using a LAI-2000 Plant Canopy Analyzer (LI-COR Inc., Lincoln, NE, USA). The dry weight of storage organs (WSO), dry weight of total above-ground biomass (TAGP) and crop height were sampled every 15 days during crop growth. Data on latent flux were measured by an eddy covariance system (EC) (Li7500 & CSAT3, Cambell Scientific, USA) that was installed here for long-term use at a height of 2.85 m. The correction of EC data was produced with revised EdiRE software from the University of Edinburgh (Xu et al., 2008). Nitrogen (329 kg ha^{-1}),

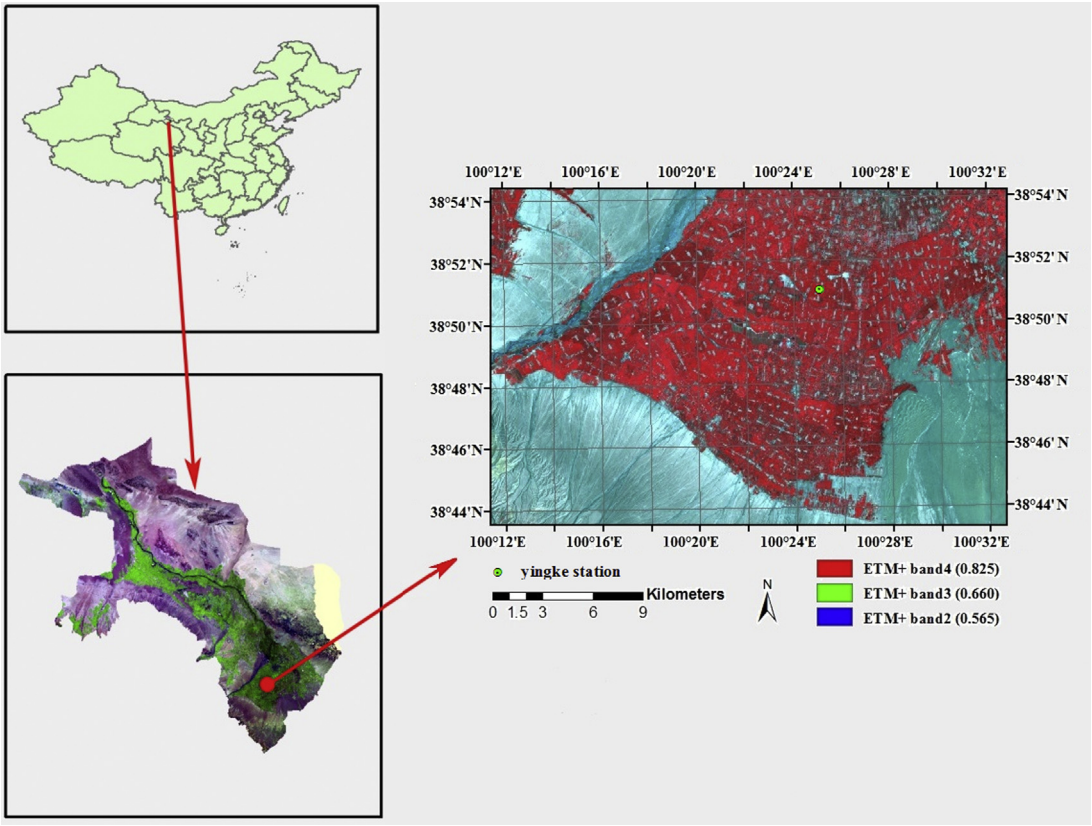

Fig. 1. Study region.

potassium (220 kg ha^{-1}) and phosphorus (87 kg ha^{-1}) fertilizers were applied to the maize fields throughout the growth period.

2.3. Remote sensing data

Sensors onboard the Landsat satellite series provide an unparalleled data source for land surface mapping and monitoring (Byrne et al., 1980; Cohen and Goward, 2004; Hansen et al., 2008; Healey et al., 2005; Masek et al., 2008; Vogelmann et al., 2001). Landsat sensors provide long-term, repeated, global coverage (1972–present) at relatively high spatial resolutions (30 m for the TM, ETM+ and OLI sensors; 80 m for the MSS sensors). In this study, we used the ETM+ dataset (L1T product for path 133, row 33) provided by the Geospatial Data Cloud, Computer Network Information Centre, Chinese Academy of Sciences (http://www.gscloud.cn). Four L1T ETM+ images, which were captured on cloud-free days that covered the full maize growth period, were selected for use in our model (Table 1). The L1T ETM+ data were geometrically corrected using ground control points and topographically corrected using a digital elevation model. Atmospheric correction was applied using the Fast Line-of-sight Atmospheric Analysis of Spectral Hypercubes (FLAASH) model in ENVI (RSI, 2001).

2.4. The coupled hydrology-crop growth model

In this study, we used a coupled hydrology-crop growth model first presented elsewhere (Li et al., 2012). The dynamic crop growth model WOFOST (Boogaard et al., 1998) and the hydrological model used to simulate water flow and root water uptake in unsaturated zones HYDRUS-1D (Šimůnek et al., 2005) were linked through an indicator for the degree of water stress, which was defined as the ratio between actual water uptake rate and potential transpiration rate. The basic coupling process is shown in Fig. 2: ① The irrigation and precipitation, the daily net radiation, the daily maximum and minimum temperatures, the daily wind speed and the daily relative humidity are the input terms in the HYDRUS model. ② The potential evaporation and transpiration are calculated by the Penman-Monteith combination method (Monteith, 1965; Monteith, 1981) in the HYDRUS model. ③ The water uptake is calculated according to Feddes equation (Feddes et al., 1978) in the HYDRUS model. ④ The soil water balance, soil moisture and groundwater depth are calculated using the HYDRUS model. ⑤ The root water uptake and actual transpiration on a daily basis are assumed the same, because most root water uptake is consumed by crop transpiration. Therefore, the ratio between calculated actual water uptake based on Feddes equation and potential transpiration based on Penman-Monteith method is regarded as an indicator for the degree of water stress. ⑥ The potential daily total gross CO_2 assimilation of the crop, which is calculated according to the WOFOST model, is multiplied by the water stress ratio to calculate the actual daily CO_2 assimilation. Then, carbohydrate allocation among different crop parts is calculated according to the WOFOST model. ⑦ The calculated vegetation parameters from the WOFOST model, more specifically rooting depth, height of the crop and LAI, are then used as inputs for the HYDRUS model at the next step.

Through this framework, the modules were fully coupled at a daily time step. Two types of parameter sets were required to run the coupled hydrology-crop growth model: (1) crop parameters from WOFOST and (2) soil parameters from HYDRUS. A detailed description of this coupled model can be found in Li et al. (2012).

2.5. Sensitivity analysis

A global sensitivity analysis of the coupled hydrology-crop growth model has been implemented with the EFAST method using

Table 1
Information of selected ETM+ images.

Passing date	Path	Raw	Center location (°)	Solar azimuth (°)	Solar elevation (°)	Mean cloudiness (%)
2008-5-12	133	33	38.86N, 100.62E	130.9	61.8	1.2
2008-5-28	133	33	38.87N, 100.62E	125.8	64.2	0.36
2008-7-15	133	33	38.90N, 100.63E	122.5	62.7	7.6
2008-8-16	133	33	38.93N, 100.63E	133.2	56.9	17.3

a SimLab Dynamic Link Library (http://simlab.jrc.ec.europa.eu/). Only model parameters were analyzed. Neither input variables nor the initial conditions of the coupled model take part in the sensitivity analysis. The appropriate ranges for the input factors used in the sensitivity analysis were defined based on values from a literature review, experience, and research objectives as well as the default, minimum, and maximum values used in the WOFOST and HYDRUS databases. Uniform distributions were assigned to input factors when only the base value was known and when the range was considered finite if no explicit knowledge of the input factor's distribution was available (McKay, 1995). This conservative assumption allowed for an equal probability of occurrence for the input factors along the probability range (Muñoz-Carpena et al., 2010). The Monte Carlo sample size was set to 5000 for each factor. The parameters were divided into 11 groups according to their physical properties and functions. These parameter groups and their value ranges are shown in Table 2. A detailed description of EFAST can be found in Saltelli et al. (2000).

2.6. Coupled hydrology-crop model calibration

Because the maize characteristics (e.g. drought resistance, cold resistance, plant height, leaf width, full grain of the maize variety) for our study area were similar to those for the "grain maize 203" variety cultivated in Europe, we used the maize dataset provided by the European Community (Boons-Prins et al., 1993) to set the basic crop parameters in the model. The crop parameter groups with high first-order and interaction indices were calibrated using the FSEOPT optimization algorithm developed by Stol et al. (1992). The default values in the basic parameter dataset were used for all other parameters (MAG 203). Two parameters related to temperature accumulation, the temperature sum from emergence to anthesis (TSUM1), and the temperature sum from anthesis to maturity (TSUM2) were calculated by adding the daily average temperatures (which were above 0 °C; biological zero point) from the collected meteorological data.

The soil hydraulic parameters, including saturated water content θ_s ($L^3 L^{-3}$), residual water content θ_r ($L^3 L^{-3}$), saturated hydraulic conductivity K_s ($L T^{-1}$), the air entry parameter α, the pore size distribution parameter n, and the pore connectivity parameter l, were obtained from previous research (Li et al., 2012).

2.7. Ensemble Kalman filter

The EnKF algorithm, proposed by Evensen (1994) and later improved by Burgers et al. (1998), is based on Monte Carlo or ensemble generations, where the approximation of an a priori state error covariance matrix is forecasted by propagating an ensemble

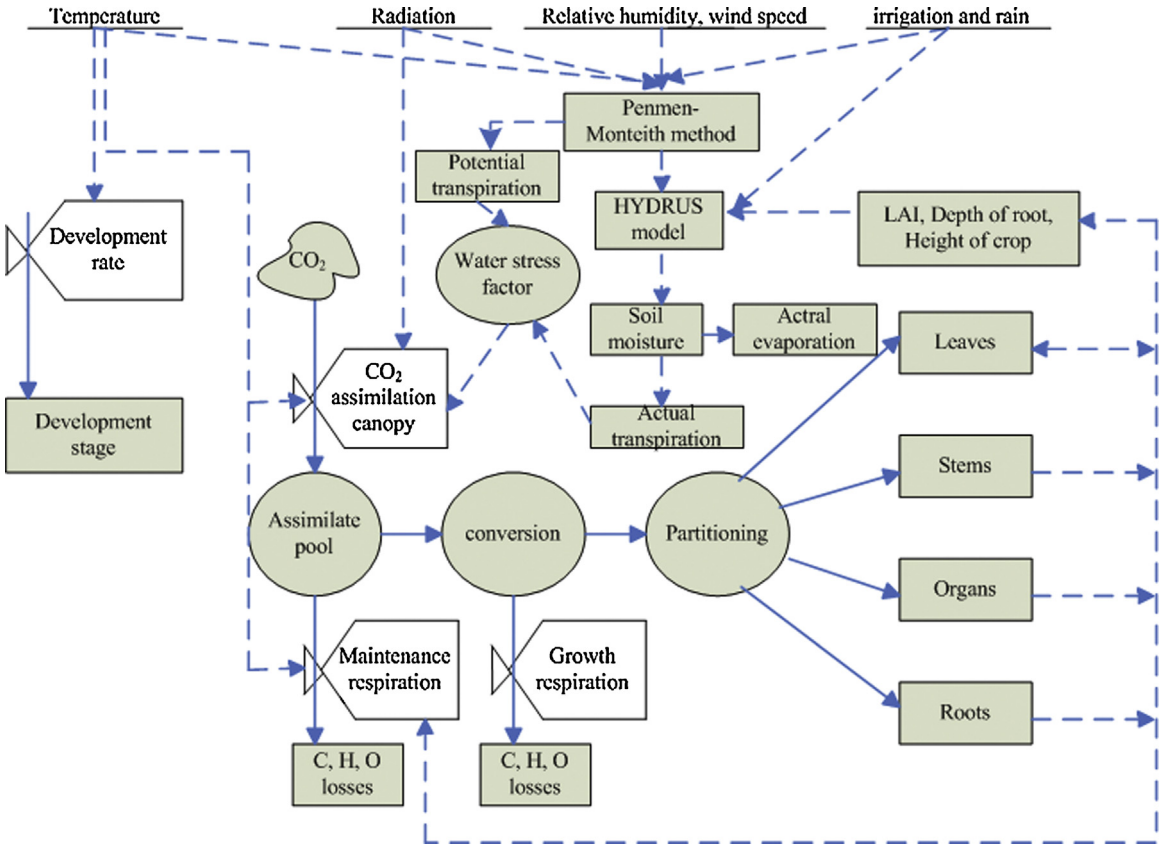

Fig. 2. Illustration of the coupled hydrology-crop growth model.

Table 2
The groups of parameters and the value ranges of parameters for EFAST.

Group	Parameter	Meaning	Unit	Values range
Soil hydraulic parameters (HYDRUS)	Parameters of HYDRUS model	Soil hydraulic parameters	($cm^3\ cm^{-3}$) ($cm^3\ cm^{-3}$) – – ($cm\ d^{-1}$)	θ_r U(0.01–0.1) θ_s U(0.25–0.4) a U(0.02–0.14) n U(0.1–0.6) K_s U(10–800)
Emergence	TBASEM TEFFMX	Lower threshold temperature for emergence Maximum effective temperature for emergence	(°C) (°C)	U(2–5) U(20–30)
Phenology	TSUM1 TSUM2	Thermal time from emergence to anthesis Thermal time from anthesis to maturity	(°C d) (°C d)	U(700–900) U(800–1200)
LAI	RGRLAI LAIEM	Maximum relative increase in LAI Leaf area index at emergence	($ha\ ha^{-1}\ d^{-1}$) ($ha\ ha^{-1}$)	U(0.01–0.04) U(0.01–0.03)
Green area	SPAN SLATB SLATB1	Life span of leaves growing at 35 °C Specific leaf area as a function of development stage Specific leaf area as a function of development stage	(d) ($ha\ kg^{-1}$) ($ha\ kg^{-1}$)	U(30–36) U(0.002–0.003) U(0.001–0.002)
Assimilation	AMAXTB AMAXTB1 AMAXTB2 AMAXTB3 AMAXTB4	Maximum leaf CO_2 assimilation rate at development stage of the crop growth Maximum leaf CO_2 assimilation rate at the first development stage of the crop maturity Maximum leaf CO_2 assimilation rate at the second development stage of the crop maturity Maximum leaf CO_2 assimilation rate at the third development stage of the crop maturity Maximum leaf CO_2 assimilation rate at the fourth development stage of the crop maturity	($kg\ ha^{-1}\ h^{-1}$) ($kg\ ha^{-1}\ h^{-1}$) ($kg\ ha^{-1}\ h^{-1}$) ($kg\ ha^{-1}\ h^{-1}$) ($kg\ ha^{-1}\ h^{-1}$)	U(50–70) U(50–70) U(50–70) U(30–50) U(0–25)
Conversion of assimilates into biomass	CVO CVS CVL CVR	Conversion efficiency of assimilates into storage organ Conversion efficiency of assimilates into stem Conversion efficiency of assimilates into leaf Conversion efficiency of assimilates into root	($kg\ kg^{-1}$) ($kg\ kg^{-1}$) ($kg\ kg^{-1}$) ($kg\ kg^{-1}$)	U(0.6–0.8) U(0.59–0.76) U(0.61–0.75) U(0.62–0.76)
Maintenance respiration	RMS RML Q10 RMO RMR	Relative maintenance respiration rate stems Relative maintenance respiration rate leaves Relative change in respiration rate per 10 °C temperature change Relative maintenance respiration rate storage organs Relative maintenance respiration rate roots	($kg(CH_2O)\ kg^{-1}\ d^{-1}$) ($kg(CH_2O)\ kg^{-1}\ d^{-1}$) ($kg(CH_2O)\ kg^{-1}\ d^{-1}$) ($kg(CH_2O)\ kg^{-1}\ d^{-1}$)	U(0.013–0.02) U(0.027–0.033) U(1.6–2) U(0.005–0.015) U(0.01–0.016)
Death rates due to water stress	PERDL	Maximum relative death rate of leaves due to water stress	($kg\ kg^{-1}\ d^{-1}$).	U(0.02–0.06)
Correction factor transpiration rate	CFET	correction factor transpiration rate		U(0.7–1.2)
Root parameters	RRI RDI RDMCR	Maximum daily increase in rooting depth Initial rooting depth maximum rooting depth	($cm\ d^{-1}$) (cm) (cm)	U(2–3) U(7–14) U(90.5–120)

of model states using updated states (ensemble members) from the previous time step. The EnKF algorithm generates the ensemble of observations at each update time by introducing noise drawn from a distribution with mean equal to zero and covariance equal to the observational error covariance matrix (Burgers et al., 1998; Reichle et al., 2002a,b). The EnKF algorithm has been widely applied to land data assimilation systems (Reichle et al., 2002b; de Wit and Van Diepen, 2007; Li et al., 2007; Huang et al., 2008; Jin and Li, 2009).

The basic equation for the EnKF algorithm can be defined according to the following equation:

$$A^{a} = A + P_e H^{T}(HP_e H^{T} + R_e)^{-1}(D - HA), \quad (1)$$

where A_a and A are the analysis and forecast matrices, respectively, for the state variable ensembles; D represents the observation vector; P_e and R_e are the covariance matrices for the state and observation variables, respectively; H is a measurement operator; and $(D - HA)$ are the innovation vectors.

In this study, the simulated value for LAI was the only state variable that was directly assimilated from external observations (i.e. through the ETM+ dataset). Because the observation operator H was an identity matrix and because no other observations were involved, Eq. (1) can be rewritten as the following equation:

$$A_i^{a} = A_i + \frac{P_e}{(P_e + R_e)}(D_i - A_i), \quad (2)$$

where A_i^{a} and A_i are the analyzed and forecasted LAI states, respectively, for ensemble member i; P_e and R_e are the covariances for the modelled and observed LAI values, respectively; and D_i is the perturbed LAI observation, which is used to update ensemble member

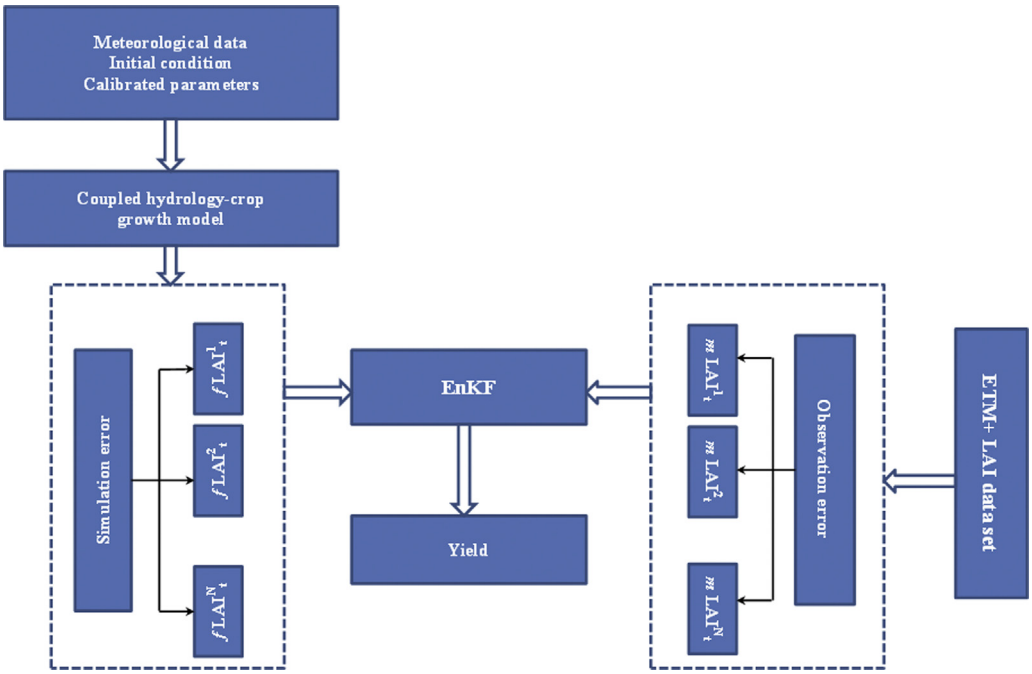

Fig. 3. Flowchart of the EnKF assimilation of ETM+ LAI.

i (Burgers et al., 1998). Note that, for the simultaneous assimilation of multiple observations (e.g. soil moisture and LAI), Eq. (1) should be used. A detailed description of this algorithm can be found in Evensen (2003).

A flowchart for regional maize yield estimates made through the EnKF-assisted assimilation of ETM+ LAI data into the coupled hydrology-crop growth model is illustrated in Fig. 3. The EnKF-assisted assimilation was performed independently per grid unit at a 30 m resolution. The coupled crop model was initialized at the sowing date. The ensemble size was set at 100 according to the recommendations of other researchers (de Wit and Van Diepen, 2007).

On the first day of simulation, white Gaussian noise was added to shift the simulated LAI and to generate the first ensemble for the forecasted LAI $\{fLAI^1, fLAI^2, \ldots, fLAI^N\}$. If there were observation data for time t, we added a Gaussian perturbation-ensemble to the observation LAI to generate an observation ensemble $\{mLAI^1, mLAI^2, \ldots, mLAI^N\}$. The forecasted ensemble and the observation ensemble were then assimilated to obtain the optimal estimate ensemble $\{LAI^1, LAI^2, \ldots, LAI^N\}$, which was added to the coupled hydrology-crop growth model to obtain the forecast ensemble for time $t+1$. If an observation LAI did not exist for time t, the forecast ensemble was added to the coupled hydrology-crop growth model directly. This process was repeated until crop maturation occurred. The mean of the optimal estimate ensemble was the best estimate of LAI at time t, which was ultimately added to the coupled crop growth model to estimate the maize yield for each grid.

2.8. LAI extraction from ETM+ images

A time series of NDVI values can supply information on crop growth status for different crops over different growth periods. Thus, the characteristics of the maize cultivating region were reflected in the false colour composite image created from an NDVI dataset calculated from selected ETM+ images. An object-oriented feature extraction module (ENVI FX) in ENVI 5.0 was used to extract maize areas from this false colour composite image.

Numerous studies have demonstrated a strong correlation between spectral vegetation indices (SVIs) and LAI (e.g. Peterson et al., 1987; Spanner et al., 1990a,b; Colombo et al., 2003). With the available on-site LAI measurements, LAI spatial distribution maps covering the maize cultivation region for a selected date were obtained based on the regression analysis of LAI measurements and the spectral vegetation index (SVI) values. Regional LAI sampling during the crop growth period was conducted when the satellite was scheduled to pass over the region. To meet statistical requirements, 26 LAI observation samples (50% of samples) were stochastically chosen to create the LAI spatial map, and the remaining observations were reserved for validation. In this study, four SVIs (Table 3) were computed to analyze their statistical relationships with LAI. NDVI, enhanced vegetation index (EVI) (Huete et al., 1999), soil adjusted vegetation index (SAVI) (Huete, 1988), and atmospherically resistant vegetation index (ARVI) (Kaufman and Tanré, 1992) were selected as representative of intrinsic, soil adjusted and atmospherically corrected indices.

3. Results

3.1. Sensitivity analysis

The EFAST method calculates sensitivity indices from model output variance as an indicator of importance for input factors. The first-order (or main) sensitivity index for the *i*th input factor (S_i) represents the impact on model output of this factor alone. The total sensitivity index for the *i*th input factor (ST_i), the sum of all effects

Table 3
Spectral vegetation indices used in LAI retrieval. ρ_{blue}, ρ_{red}, and ρ_{nir} represent the spectral reflectance data in blue, red and infrared bands. Parameters L and γ regard respectively the canopy adjustment coefficient (the SAVI term set equal to 0.5) and atmospheric adjustment coefficient (the ARVI term set equal to 1). The coefficients adopted in the EVI formula are $C_1 = 6.0$, $C_2 = 7.5$, $C_3 = 1$, and $G = 2.5$.

SVI	Formula
NDVI	$\frac{\rho_{nir}-\rho_{red}}{\rho_{nir}+\rho_{red}}$
EVI	$EVI = G\frac{(\rho_{nir}-\rho_{red})}{\rho_{nir}+C_1\rho_{red}-C_2\rho_{blue}+C_3}$
SAVI	$SAVI = \frac{(\rho_{nir}-\rho_{red})}{(\rho_{nir}+\rho_{red}+L)}(1+L)$
ARVI	$ARVI = \frac{(\rho_{nir}-\rho_{rb})}{(\rho_{nir}+\rho_{rb})}, \quad \rho_{rb} = \rho_{red} - \gamma(\rho_{blue} - \rho_{red})$

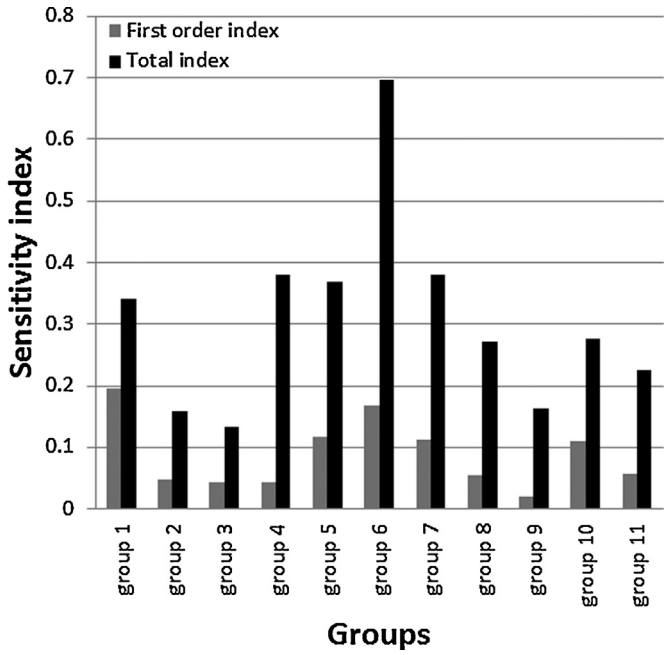

Fig. 4. Sensitivity indices of grouped parameters.

(first and higher order) involving this input factor, represents the overall impact on model output of this input factor through interactions with the others. The estimated index pairs (S_i, ST_i) are shown in Fig. 4. The results showed that five parameter groups had high first-order and total indexes including the groups containing soil hydraulic parameters, green areas, assimilation, the conversion of assimilates into biomass, and the correction factor transpiration rate. The values of the first-order and total indexes for these parameter groups were more than 0.1 and 0.27, respectively. The group of soil hydraulic parameters had the highest first-order index but a low total index, likely because the coupled model was run under realistic irrigation conditions and the water supply for crop growth was therefore adequate. The group of parameters for crop assimilation had the second highest first-order index and the highest total index. This trend can be explained by the fact that the crop assimilation process determined how many carbohydrates were allocated among different crop parts, driving the final yield of the crop. Therefore, the crop assimilation process was the most important component of crop development when water was not limited. Table 4 presents the first-order S_i and interaction indexes ($ST_i - S_i$) for each parameter group. In addition to the five parameter groups mentioned above, we also found that the group of parameters for LAI had a relatively high interaction index at 0.3.

Table 4
Sensitivity indices for each parameter group.

Group of parameters	S_i	ST_i	$ST_i - S_i$
Soil hydraulic parameters (group 1)	0.1958	0.342	0.1462
Emergence (group 2)	0.0485	0.1583	0.1098
Phenology (group 3)	0.0435	0.133	0.0895
LAI (group 4)	0.0432	0.3809	0.3377
Green area (group 5)	0.1165	0.3696	0.2531
Assimilation (group 6)	0.1674	0.6965	0.5291
Conversion of assimilates into biomass (group 7)	0.113	0.38	0.267
Maintenance respiration (group 8)	0.0541	0.2723	0.2182
Death rates due to water stress (group 9)	0.0212	0.1629	0.1417
Correction factor transpiration rate (group 10)	0.1107	0.2763	0.1656
Root parameters (group 11)	0.0569	0.2257	0.1688

3.2. Parameter estimation and validation for the coupled hydrology-crop growth model

The calibration dataset collected at Yingke station (during the maize growth period in 2008) included values for TAGP, WSO, and LAI. Table 5 shows the estimated parameters for the coupled hydrology-crop growth model, including 15 of the most sensitive crop and soil hydraulic parameters. The performance of the coupled model (Table 6) was evaluated using mean error (ME), root-mean-square error (RMSE), coefficient of variation (CV) and coefficient of determination (R^2). The RMSEs for LAI, TAGP, and WSO were 0.346 $cm^2\ cm^{-2}$, 944.8 $kg\ ha^{-1}$, and 539.8 $kg\ ha^{-1}$, respectively. The RMSEs for soil moisture in three layers (at depths of 10 cm, 40 cm and 100 cm) were 0.017 $cm^3\ cm^{-3}$, 0.02 $cm^3\ cm^{-3}$, and 0.023 $cm^3\ cm^{-3}$, respectively. The CVs for LAI, TAGP, and WSO were 13%, 6.9%, and 11%, respectively. The CVs for soil moisture in three layers (at depths of 10, 40 and 100 cm) were 6.8%, 6.9%, and 5.9%, respectively. The ME values indicated that soil moisture values were underestimated while those for LAI, TAGP, and WSO were overestimated. The R^2 value was higher than 0.8 for all parameters. ET data measured by an eddy covariance system were used to validate the coupled model. The results of this analysis are shown in Fig. 5.

3.3. LAI extraction for the study region

Because the NDVI values for maize tend to be low in May through late June, we created a false colour composite image using images from May 12 as the red band, May 28 as the green band and July 15 as the blue band. In this false colour composite image, shown in Fig. 6(a), maize appears blue, other crops appear cyan or yellow and non-crop areas appear black. The information of maize cultivating extracted by ENVI FX is shown in Fig. 6(b).

Table 7 presents the different statistical relationships between SVIs and LAI. The results indicated that the exponential relationship between NDVI and LAI had a larger determination coefficient ($R^2 = 0.7288$) compared to other statistical relationships. This exponential relationship (Fig. 7a) was validated by comparing the simulated LAI with the observed LAI (i.e. those values that were not used to determine the empirical relationship) (Fig. 7b). The RMSE and ME values for the estimated and observed LAI values were 0.51 and −0.337, respectively.

The spatial LAI maps were extracted based of the exponential relationship between NDVI and LAI for the maize crops at selected dates in our study area. LAI maps (Fig. 8) for May demonstrated that maize grew during the early growth period and that the LAI value in most pixels was lower than 1.5. An apparent increase could be seen in the LAI maps (Fig. 8) for July and August over the entire cultivated region, and the LAI value in most pixels exceeded 3.0. The mean LAI values for maps for May 12, May 28, July 15, and August 16 were 1.07, 1.29, 3.39, and 3.25, respectively. Temporal and spatial variation in LAI is generally caused by different rates of crop development or other factors resulting from the spatial heterogeneity in land surface characteristics.

3.4. Numerical experiments of LAI assimilation

Because the same maize variety was planted throughout much of the Zhangye Oasis and because soil characteristics in this region had no obvious changes, the calibrated parameter set could be assumed to be invariant in this region. However, due to differences in field management techniques (e.g. fertilization, weed control and pest control), maize tends to grow unevenly at the regional scale. As a comprehensive representation of crop status, LAI distribution was used to reflect differences in crop growth at this scale, and the EnKF algorithm integrated differences in maize

Table 5
Key parameters of the coupled hydrology-crop growth model.

Parameter	Unit	Lower limit	Upper limit	Default value	Calibrated value
SPAN	kg ha^{-1}	17.00	50.00	33.00	39.05
LAIEM	ha ha^{-1}	0.03385	0.06287	0.04836	0.04413
RGRLAI	ha ha^{-1} d^{-1}	0.0206	0.0382	0.0294	0.0281
SLATB (DVS = 0)	ha kg^{-1}	0.0018	0.0034	0.0026	0.0023
SLATB1 (DVS = 0.78)	ha kg^{-1}	0.0008	0.0016	0.0012	0.0009
AMAXTB (DVS = 0)	kg ha^{-1} h^{-1}	49.00	91.00	70.00	51.50
AMAXTB1 (DVS = 1.25)	kg ha^{-1} h^{-1}	49.00	91.00	70.00	51.19
AMAXTB2 (DVS = 1.50)	kg ha^{-1} h^{-1}	44.10	81.90	63.00	49.20
AMAXTB3 (DVS = 1.75)	kg ha^{-1} h^{-1}	34.30	63.70	49.00	58.90
AMAXTB4 (DVS = 2.00)	kg ha^{-1} h^{-1}	14.70	27.30	21.00	21.06
CVL	(kg kg^{-1})	0.6	0.76	0.68	0.656
CVO	(kg kg^{-1})	0.45	0.85	0.671	0.71
CVR	(kg kg^{-1})	0.65	0.76	0.69	0.67
CVS	(kg kg^{-1})	0.63	0.76	0.65	0.64
CFET	–	0.8	1.2	1.0	1.02
θ_r	(cm^3 cm^{-3})	0.001	0.2	–	0.05(10 cm) 0.05 (40 cm) 0.05 (100 cm)
θ_s	(cm^3 cm^{-3})	0.1	1.0	–	0.41 (10 cm) 0.41 (40 cm) 0.41 (100 cm)
α	–	0.01	0.2	–	0.08 (10 cm) 0.087 (40 cm) 0.11 (100 cm)
n	–	0.1	1	–	0.13 (10 cm) 0.115 (40 cm) 0.10 (100 cm)
K_s	(cm d^{-1})	10	1000	–	569 (10 cm) 344.85 (40 cm) 91.62 (100 cm)

Table 6
Performance of the coupled hydrology-crop growth model.

	Soil moisture (cm^3 cm^{-3})			LAI (cm^2 cm^{-2})	TAGP (kg ha^{-1})	WSO (kg ha^{-1})
Depth	10 cm	40 cm	100 cm			
R^2	0.813	0.804	0. 917	0.964	0.981	0.985
RMSE	0.017	0.02	0.023	0.346	944.8	539.8
ME	−0.003	−0.007	−0.016	0.012	933.1	415.7
CV	6.8%	6.9%	5.9%	13%	6.9%	11%

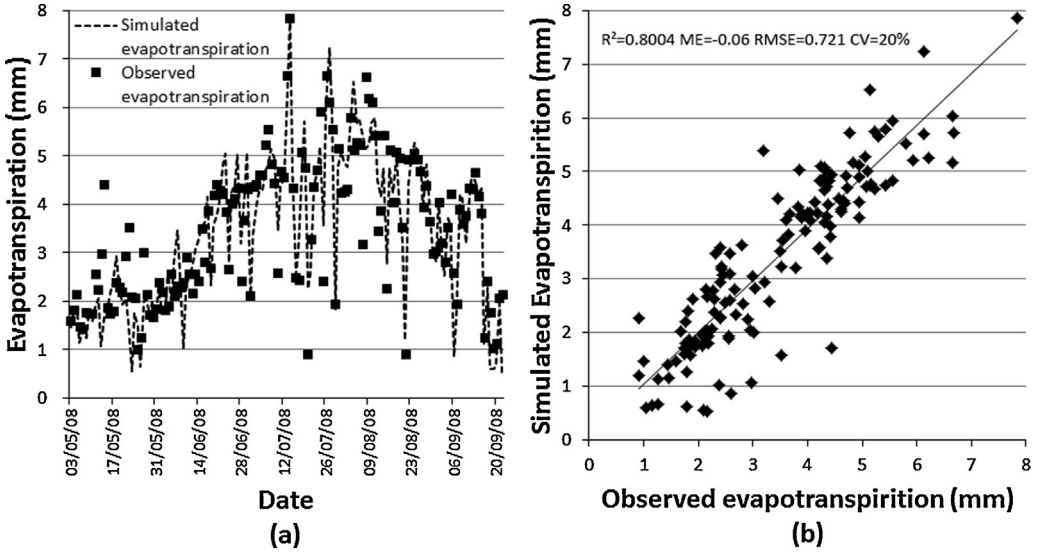

Fig. 5. Comparison of estimated evapotranspiration and observed evapotranspiration.

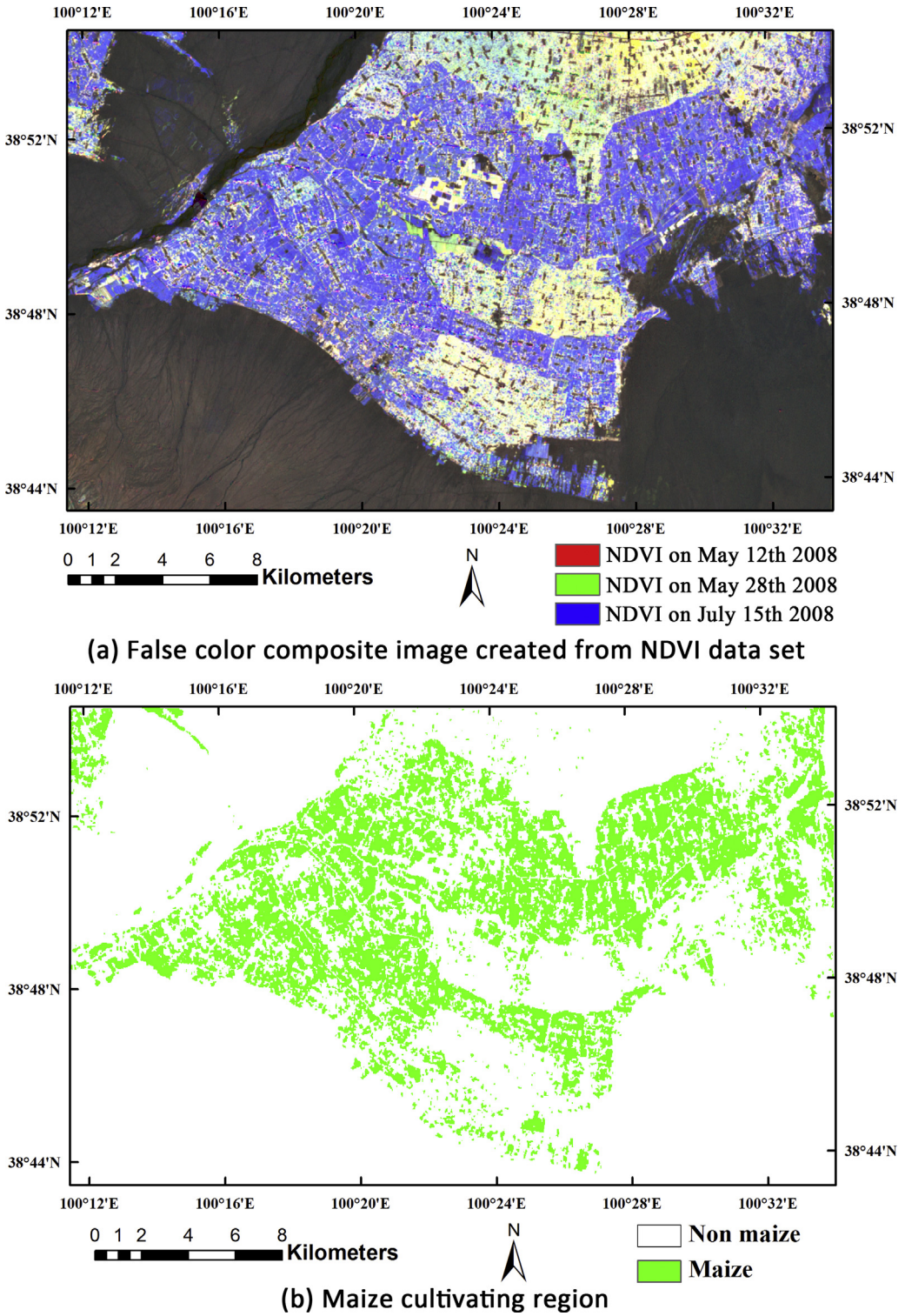

Fig. 6. Extraction of the maize cultivating region from NDVI data set.

growth rates into the coupled hydrology-crop growth model to obtain the optimal LAI profile for every maize-planting grid. The results of this analysis were evaluated based on the simulated and observed yields from fifty sample plots. A visual representation of crop growth and its spatial heterogeneities were also obtained in our LAI assimilation (Fig. 9). We found that every sample plot had a different growth curve for LAI (Fig. 9a), which also differed from the LAI evolution curve without assimilation. In general, the EnKF algorithm can influence the LAI simulation by the updating strategy. According to the different simulation trajectories obtained in the sample plots, the final yields for each sample plot are shown in Fig. 9b. The RMSE, ME, and CV for the sample yield were 747.2, −546.17 kg ha^{-1}, and 8.7%, respectively. The integration of the crop growth model and remote sensing observations provided a strong approach for estimating the regional crop yield.

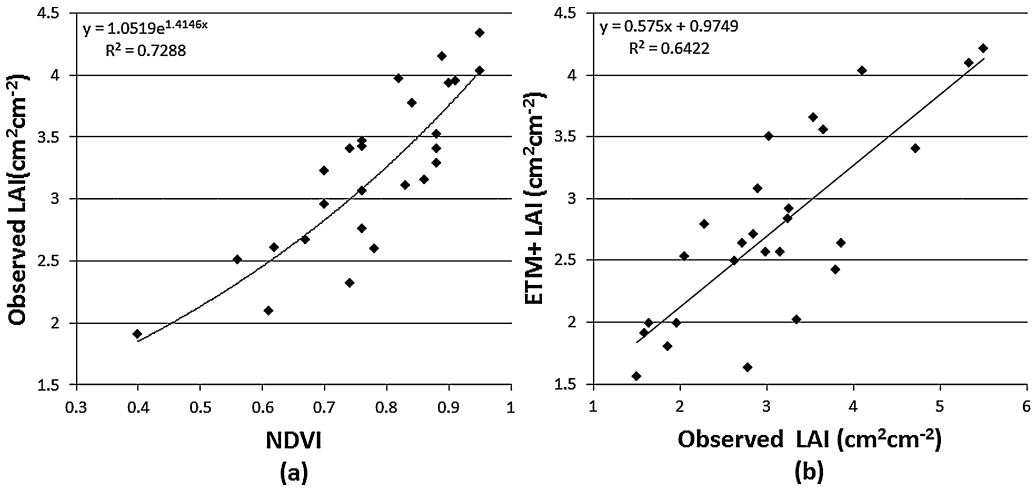

Fig. 7. The statistical model between the observed LAI and ETM+ NDVI (a) and model evaluation (b).

Table 7
Statistical relationships between SVIs and LAI.

NDVI	R^2	EVI	R^2
$y = 1.05e^{1.41x}$	0.7288	$y = 2.03e^{1.12x}$	0.4887
$y = 4.21x - 0.05$	0.7024	$y = 3.45x + 1.86$	0.5061
$y = 2.77\ln(x) + 3.97$	0.6576	$y = 1.33\ln(x) + 4.54$	0.5075
$y = 3.96x^2 - 1.44x + 1.89$	0.722	$y = -3.16x^2 + 6.05x + 1.38$	0.5107
$y = 4.06x^{0.94}$	0.7029	$y = 4.85x^{0.43}$	0.5005
SAVI	R^2	**ARVI**	R^2
$y = 2.21e^{0.31x}$	0.1987	$y = 1.27e^{1.41x}$	0.6821
$y = 0.99x + 2.1$	0.2174	$y = 4.35x + 0.41$	0.7054
$y = 0.48\ln(x) + 3.19$	0.0805	$y = 2.6\ln(x) + 4.41$	0.6806
$y = 3.02x^2 - 4.69 + 4.42$	0.6059	$y = 2.34x^2 + 1.4x + 1.3$	0.7091
$y = 3.12x^{0.15}$	0.0703	$y = 4.64x^{0.85}$	0.6643

3.5. Regional yield estimation after assimilating extracted ETM+ LAI data

The EnKF algorithm was applied to each pixel to calibrate the model trajectory and to estimate the maize yield in the study region. All LAI maps were integrated into the coupled hydrology-crop growth model, and we obtained a spatially distributed yield for the study region at a spatial resolution similar to that of ETM+ data. The spatial distribution of the regional maize yield is presented in Fig. 10. In typical regions, maize yields generally do not exceed 8600.00 kg ha^{-1}. Throughout most of the Zhangye Oasis, maize yields ranged from 6500.00 to 8000.00 kg ha^{-1}, which occupied 89.9% of the maize planting region. A total of 17.7% of the planted areas experienced yields that ranged from 7000.00 to 7500.00 kg ha^{-1}, and 60.8% of the planted areas had yields from

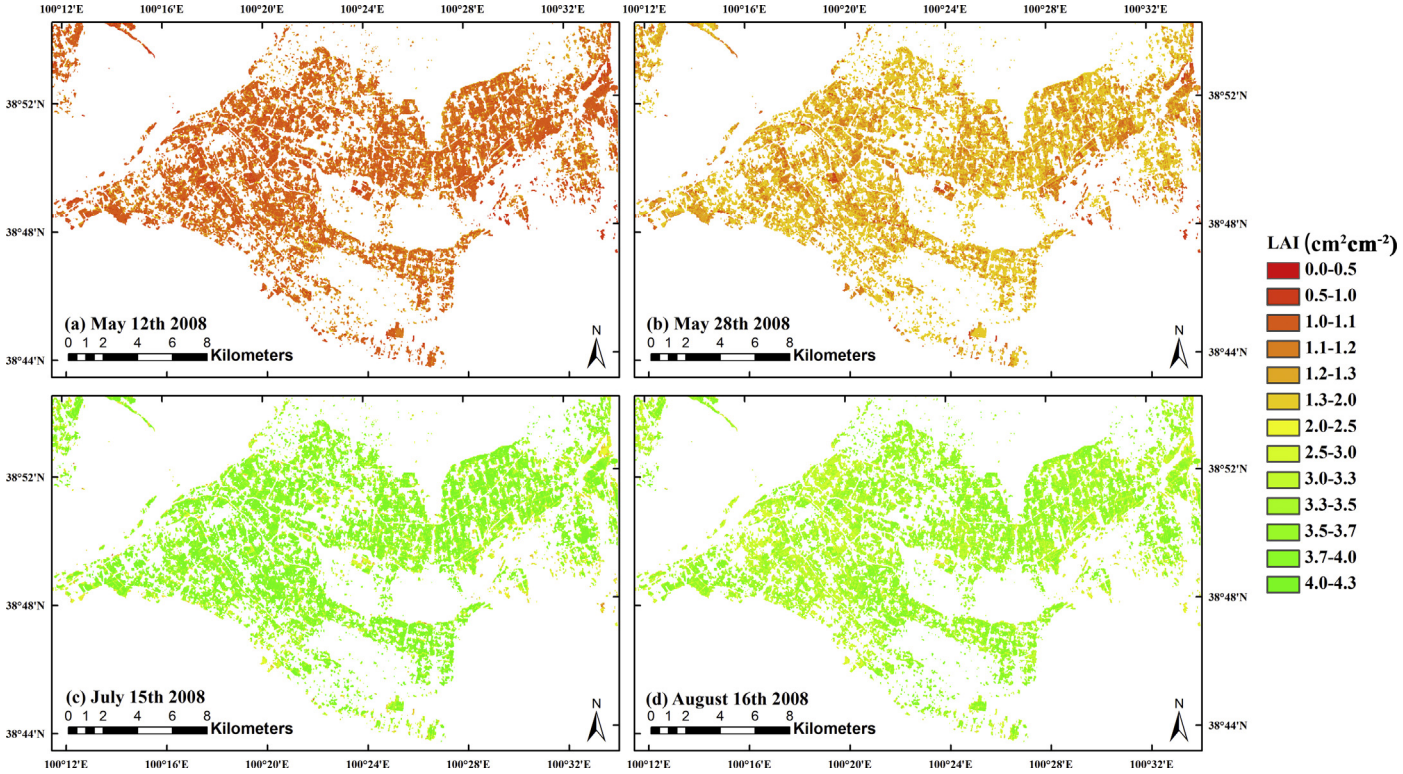

Fig. 8. LAI distribution maps for maize cultivating region.

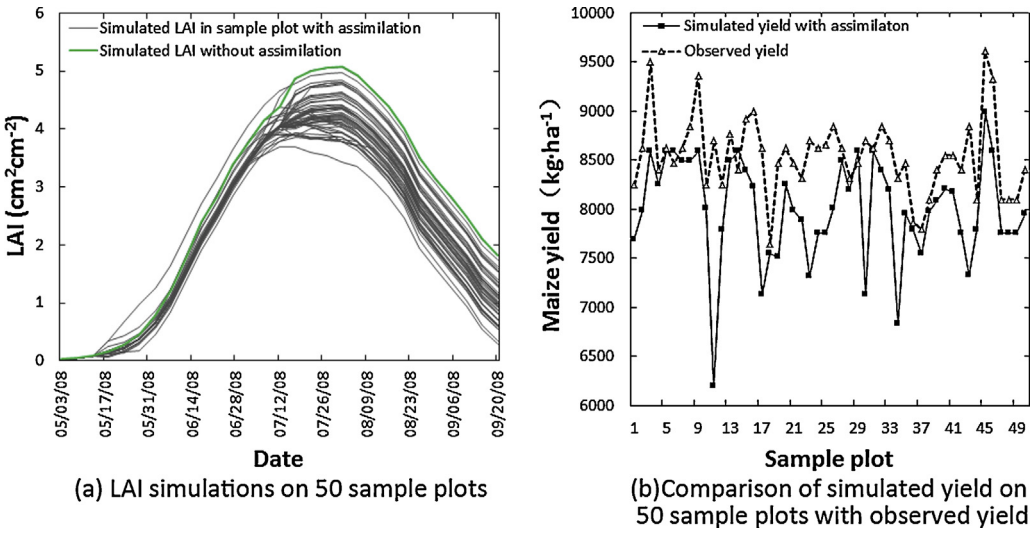

Fig. 9. Simulated LAI on 50 sample plots after assimilation (a) and comparison of observed yield with the simulated yield (after assimilation of LAI) on 50 sample plots (b).

7500.00 to 8000.00 kg ha^{-1}. The minimum, maximum and mean yields were 6502, 8590 and 7596 kg ha^{-1}, respectively. In regions where the yield was below the mean value, the crops could have suffered from water stress, plant disease or insect pests. In contrast with the coupled hydrology-crop growth model alone, the integrated approach was able to obtain the spatial distribution and regional variation in crop yield.

4. Discussion and conclusions

The objective of this study was to develop a method that could supply the impacts of irrigation, fertilizer application, and field management on variations in maize yield at a regional scale. For this purpose, the EnKF algorithm was developed to integrate regional ETM+ LAI data with a high spatial resolution into a fully coupled hydrology-crop growth model to obtain the spatial distribution and regional variation in maize yield. The assimilation results were evaluated using the yield observations collected from sample plots. The results showed that the assimilation of remote sensing data into the coupled hydrology-crop growth model provided a relatively precise, region-wide spatial distribution for maize yield in the Zhangye Oasis. This method has great potential for regional crop yield estimates.

In this study, only the maize yield was estimated for study region. The maize cultivation region was effectively extracted from a false colour composite image created from an ETM+ NDVI data set. However, when applied to a wider scale such as a watershed, the crop species are miscellaneous. Accurate crop classifications are critical for the correct determination of temporal and spatial LAI crop distributions. Our future studies will focus on the extraction of crop planting structures, which is an essential step toward operational regional yield predictions.

Based on *in situ* LAI observations, LAI distribution maps can be obtained from the statistical relationship between SVI and LAI.

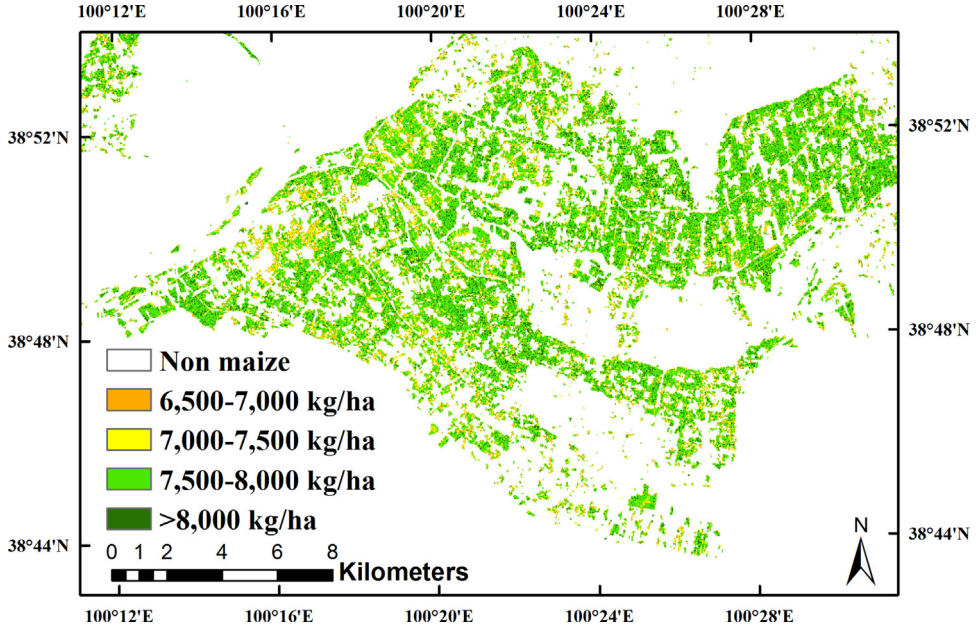

Fig. 10. Spatial distribution of the maize yields after assimilation.

However, due to the lower temporal resolution of the ETM+ data, the temporal mismatch between the ETM+ data and ground LAI observations will induce errors in the extraction of the LAI map. An improved retrieval algorithm, such as the canopy radiative transfer model, will also be integrated into the coupled hydrology-crop growth model; and multi-source remote sensing data at a multi-temporal and multi-spatial resolution, such as microwave data, will also be used to avoid the disadvantages inherent in optical remote sensing (Dente et al., 2008).

Only LAI was assimilated for yield estimates. When evapotranspiration or/and soil moisture can be derived from field measurements or remotely sensing data, a multi-objective assimilation algorithm based on the coupled hydrology-crop growth model and the EnKF could be applied to simulate different impacts on yield formation in the future. Furthermore, the use of alternative assimilation algorithms, such as the ensemble Kalman smoother or 4D-VAR, could be explored, and different kinds of approaches could be combined to more accurately determine regional crop yields.

Acknowledgements

This work was supported by NSFC (National Science Foundation of China, grant number: 91125023), Gansu Sci. & Tech. Program (grant number: 1204WCGA013), the Fundamental Research Funds for the Central Universities (grant number: lzujbky-2013-44) and SSSTC (Sino Swiss Science and Technology Cooperation Program, grant number: IP14-092010). Gratitude is expressed to the Environmental and Ecological Science Data Center in West China for providing data.

References

Anwar, M.R., McKenzie, B.A., Hill, G.D., 2003. Water-use efficiency and the effect of water deficits on crop growth and yield of kabuli chickpea (*Cicer arietinum* L.) in a cool-temperate subhumid climate. J. Agric. Sci. 141, 285–301.

Boogaard, H.L., Van Diepen, C.A., Rötter, R.P., Cabrera, J.C.M.A., Van Laar, H.H., 1998. WOFOST 7.1: User's Guide for the WOFOST 7.1 Crop Growth Simulation Model and WOFOST Control Center 1.5, Techn. Doc. 52. Alterra, WUR, Wageningen, The Netherlands, pp. 144.

Boons-Prins, E.R., de Koning, G.H.J., Van Diepen, C.A., Penning de Vries, F.W.T., 1993. Crop specific simulation parameters for yield forecasting across the European Community, Simulation Reports CABO-TT 32, CABO-DLO, DLO Winand Staring Centre, JRC, Wageningen.

Bouman, B.A.M., Kropff, M.J., Tuong, T.P., Wopereis, M.C.S., Ten Berge, H.F.M., Van Laar, H.H., 2001. ORYZA2000: Modeling Lowland Rice. IRRI/Wageningen University.

Burgers, G., van Leeuwen, P.J., Evensen, G., 1998. Analysis scheme in the ensemble Kalman filter. Mon. Wea. Rev. 126, 1719–1724.

Byrne, G.F., Crapper, P.F., Mayo, K.K., 1980. Monitoring land-cover change by principal component analysis of multi-temporal Landsat data. Remote Sens. Environ. 10, 175–184.

Casanova, J.J., Judge, J., 2008. Estimation of energy and moisture fluxes for dynamic vegetation using coupled SVAT and crop-growth models. Water Resour. Res. 44, W07415, http://dx.doi.org/10.1029/2007WR006503.

Chen, S.N., Zhao, Y.X., Shen, S.H., 2012. Applicability of PyWOFOST model based on ensemble Kalman filter in simulating maize yield in Northeast China. Chin. J. Agrometeor. 33 (2), 245–253.

Chipnashi, A.C., Ripley, E.A., Lawford, R.G., 1999. Large-scale simulation of wheat yields in a semi-arid environment using crop-growth model. Agric. Syst. 59, 57–66.

Cohen, W.B., Goward, S.N., 2004. Landsat's role in ecological applications of remote sensing. Bioscience 54, 535–545.

Colombo, R., Bellingeri, D., Fasolini, D., Marino, C.M., 2003. Retrieval of leaf area index in different vegetation types using high resolution satellite data. Remote Sens. Environ. 86 (1), 120–131.

Curnel, Y., de Wit, A.J.W., Duveiller, G., Defourny, P., 2011. Potential performances of remotely-sensed LAI assimilation in WOFOST model based on an OSS experiment. Agric. For. Meteorol. 151, 1843–1855.

Dente, L., Satalino, G., Mattia, F., Rinaldi, M., 2008. Assimilation of leaf area index derived from ASAR and MERIS data into CERES-Wheat model to map wheat yield. Remote Sens. Environ. 112 (4), 1395–1407.

de Wit, A., Van Diepen, K., 2007. Crop model data assimilation with the ensemble Kalman filter for improving regional crop yield forecasts. Agric. For. Meteorol. 146, 38–56.

de Wit, A., Duveillerb, G., Defournyc, P., 2012. Estimating regional winter wheat yield with WOFOST through the assimilation of green area index retrieved from MODIS observations. Agric. For. Meteorol. 164, 39–52.

Dorigo, W.A., Zurita-Milla, R., de Wit, A.J.W., Brazile, J., Singh, R., Schaepman, M.E., 2007. A review on reflective remote sensing and data assimilation techniques for enhanced agroecosystem modeling. Int. J. Appl. Earth Observ. Geoinform. 9 (2), 165–193.

Evensen, G., 1994. Sequential data assimilation with a nonlinear quasi-geostrophic model using Monte Carlo methods to forecast error statistics. J. Geophys. Res. 99, 10143–10162.

Evensen, G., 2003. The ensemble Kalman filter: theoretical formulation and practical implementation. Ocean Dyn. 53 (4), 343–367.

Eitzinger, J., Trnka, M., Hösch, J., Zalud, Z., Dubrovsky′, M., 2004. Comparison of CERES, WOFOST and SWAP models in simulating soil water content during growing season under different soil conditions. Ecol. Modell. 171, 223–246.

Fang, H.L., Liang, S.L., Hoogenboom, G., 2011. Integration of MODIS LAI and vegetation index products with the CSM-CERES-Maize model for corn yield estimation. Int. J. Remote Sens. 32 (4), 1039–1065.

Feddes, R.A., Kowalik, P.J., Zaradny, H., 1978. Simulation of Field Water Use and Crop Yield, Simulation Monograph. Pudoc, Wageningen, The Netherlands, pp. 9–30.

Hansen, M.C., Roy, D.P., Lindquist, E., Adusei, B., Justice, C.O., Altstatt, A., 2008. A method for integrating MODIS and Landsat data for systematic monitoring of forest cover and change in the Congo Basin. Remote Sens. Environ. 112, 2495–2513.

Healey, S.P., Cohen, W.B., Yang, Z.Q., Krankina, O.N., 2005. Comparison of Tasseled Cap-based Landsat data structures for use in forest disturbance detection. Remote Sens. Environ. 97, 301–310.

Huang, C.L., Li, X., Lu, L., 2008. Experiments of one-dimensional soil moisture assimilation system based on ensemble Kalman filter. Remote Sens. Environ. 112, 888–900.

Huete, A.R., 1988. A soil adjusted vegetation index (SAVI). Remote Sens. Environ. 25, 295–309.

Huete, A.R., Justice, C.O., van Leeuwen, W., 1999. MODIS Vegetation Index (MOD 13) Algorithm Theoretical Basis Document (ATBD-MOD-13) version 3, available at http://eospso.gsfc.nasa.gov/ftp_ATBD/REVIEW/MODIS/ATBD_MOD_13/atbd_mod_13.pdf

Jin, H., Wang, J., Xiao, Z., Fu, Z., 2010. Leaf area index estimation from MODIS data using the ensemble Kalman smoother method. In: 2010 IEEE International Geoscience and Remote Sensing Symposium, pp. 260–263.

Jin, R., Li, X., 2009. Improve the estimation of hydrothermal state variables in the active layer of frozen ground by assimilating in situ observations and SSM/I data. Sci. China Ser. D: Earth Sci. 52 (11), 1732–1745.

Kaufman, Y.J., Tanré, D., 1992. Atmospherically resistant vegetation index (ARVI) for EOS-MODIS. IEEE Trans. Geosci. Remote Sens. 30, 261–270.

Kogan, F.N., 1998. Global drought and flood-watch from NOAA polar-orbitting satellites. Adv. Space Res. 21 (3), 477–480.

Kropff, M.J., Teng, P.S., Aggarwal, P.K., Bouman, B., Bouma, J., Van Laar, H.H., 1996. Applications of Systems Approaches at the Field Level, vol. 2. Kluwer Academic Publishers, The Netherlands, pp. 465.

Li, X., Huang, C., Che, T., Jin, R., Wang, S., Wang, J., Gao, F., Zhang, S., Qiu, C., Wang, C., 2007. Development of a Chinese land data assimilation system: its progress and prospects. Prog. Nat. Sci. 17 (8), 881–892.

Li, X., Li, X., Li, Z., Ma, M., Wang, J., Xiao, Q., Liu, Q., Che, T., Chen, E., Yan, G., Hu, Z., Zhang, L., Chu, R., Su, P., Liu, Q., Liu, S., Wang, J., Niu, Z., Chen, Y., Jin, R., Wang, W., Ran, Y., Xin, X., Ren, H., 2009. Heihe watershed allied telemetry experimental research. J. Geophys. Res. 114 (D22103), http://dx.doi.org/10.1029/2008JD011590

Li, Y., Kinzelbach, W., Zhou, J., Cheng, G., Li, X., 2012. Modelling irrigated maize with a combination of coupled-model simulation and uncertainty analysis, in the northwest of China. Hydrol. Earth Syst. Sci. 16, 1465–1480, http://dx.doi.org/10.5194/hess-16-1465-2012.

Liang, S., Qin, J., 2008. Data assimilation methods for land surface variable estimation. In: Liang, S. (Ed.), Advances in Land Remote Sensing: System, Modeling, Inversion and Application. Springer, New York, pp. 319–339.

Liu, W.T., Kogan, F., 2002. Monitoring Brazilian soybean production using NOAA/AVHRR based vegetation condition indices. Int. J. Remote Sens. 23 (6), 1161–1179.

Ma, G., Huang, J., Wu, W., Fan, J., Zou, J., Wu, S., 2012. Assimilation of MODIS-LAI into the WOFOST model for forecasting regional winter wheat yield. Math. Comput. Modell. 58, 634–643.

Ma, H., Huang, J., Zhu, D., Liu, J., Su, W., Zheng, C., Fan, J., 2013. Estimating regional winter wheat yield by assimilation of time series of HJ-1 CCD NDVI into WOFOST–ACRM model with Ensemble Kalman Filter. Math. Comput. Modell. 58, 759–770.

Maruyama, A., Kuwagata, T., 2010. Coupling land surface and crop growth models to estimate the effects of changes in the growing season on energy balance and water use of rice paddies. Agric. For. Meteorol. 150 (7), 919–930.

Masek, J.G., Huang, C.Q., Wolfe, R., Cohen, W., Hall, F., Kutler, J., Nelson, P., 2008. North American forest disturbance mapped from a decadal Landsat record. Remote Sens. Environ. 112, 2914–2926.

Matthews, R.B., Stephens, W., 2002. Crop-soil Simulation Models, Applications in Developing Countries. CABI, Publishing, Wallingford, United Kingdom, pp. 277.

McKay, M.D., 1995. Evaluating Prediction Uncertainty. NUREG/CR-6311. US Nuclear Regulatory Commission and Los Alamos National Laboratory, Los Alamos, NM.
Mignolet, C., Schott, C., Benoît, M., 2007. Spatial dynamics of farming practices in the Seine basin: methods for agronomic approaches on a regional scale. Sci. Total Environ. 375, 13–32.
Monteith, J.L.,1965. Evaporation and environment. In: Proceedings of the 19th Symposium of the Society for Experimental Biology. Cambridge University Press, New York, pp. 205–233.
Monteith, J.L., 1981. Evaporation and surface temperature. Quart. J. Royal Soc. 107, 1–27.
Moulin, S., Guerif, M., 1999. Impacts of model parameter uncertainties on crop reflectance estimates: a regional case study on wheat. Int. J. Remote Sens. 20 (1), 213–218.
Muñoz-Carpena, R., Fox, G.A., Sabbagh, G.J., 2010. Parameter importance and uncertainty in predicting runoff pesticide reduction with filter strips. J. Environ. Qual. 39 (1), 1–12.
Patil, S.L., Sheelavantar, M.N., 2004. Effect of cultural practices on soil properties, moisture conservation and grain yield of winter sorghum in semi-arid tropics of India. Hydrol. Process. 64, 49–67.
Peterson, D.L., Spanner, M.A., Running, S.W., Teuber, K.B., 1987. Relationship of thematic mapper simulator data to leaf area index of temperate coniferous forests. Remote Sens. Environ. 22 (3), 323–341.
Priesack, E., Gayler, S., Hartmann, H.P., 2006. The impact of crop growth sub-model choice on simulated water and nitrogen balances. In: Modelling Water and Nutrient Dynamics in Soil–crop Systems. Springer, Germany, pp. 183–195.
Quaife, T., Lewis, P., Kauwe, M.D., Williams, M., Law, B.E., Disney, M., Bowyer, P., 2008. Assimilating canopy reflectance data into an ecosystem model with an ensemble Kalman filter. Remote Sens. Environ. 112, 1347–1364.
Reichle, R.H., McLaughlin, D.B., Entekhabi, D., 2002a. Hydrologic data assimilation with the ensemble Kalman filter. Mon. Weather Rev. 130 (1), 103–114.
Reichle, R.H., Walker, J.P., Koster, R.D., Houser, P.R., 2002b. Extended versus ensemble Kalman filtering for land data assimilation. J. Hydrometeorol. 3 (6), 728–740.
Revill, A., Sus, O., Barrett, B., Williams, M., 2013. Carbon cycling of European croplands: a framework for the assimilation of optical and microwave Earth observation data. Remote Sens. Environ. 137, 84–93.
Rodriguez-Iturbe, I., Porporato, A., Laio, F., Ridolfi, L., 2001. Intensive or extensive use of soil moisture: plant strategies to cope with stochastic water availability. Geophys. Res. Lett. 28, 4495–4497.
Rouse, J.W., Haas, R.H.,1973. Monitoring Vegetation Systems in the Great Plain with ERTS. In: Third ERTS Symposium. NASA, Washington, DC, pp. 309–317.
RSI, 2001. ENVI User's Guide. September 2001 edition. Research Systems.
Saltelli, A., Chan, K., Scott, E.M., 2000. Sensitivity Analysis. Wiley Series in Probability and Statistics. Wiley, Chichester, New York.
Shepherd, A., McGinn, S.M., Wyseure, G.C.L., 2002. Simulation of the effect of water shortage on the yields of winter wheat in north-east England. Ecol. Modell. 147, 41–52.
Šimůnek, J., Van Genuchten, M.Th., Šejna, M., 2005. The HYDRUS-1D Software Package for Simulating the Movement of Water, Heat, and Multiple Solutes in Variability Saturated Media, Version 3. 0. Department of Environmental Sciences University of California Riverside, Riverside, California, USA, pp. 270.
Spanner, M.A., Pierce, L.L., Peterson, D.J., Running, S.W., 1990a. Remote sensing of temperate coniferous forest leaf area index, the influence of canopy closure, understory vegetation and background reflectance. Int. J. Remote Sens. 11 (l), 95–111.
Spanner, M.A., Pierce, L.L., Running, S.W., Peterson, D.L., 1990b. The seasonality of AVHRR data of temperate coniferous: relationship with leaf area index. Remote Sens. Environ. 33, 97–112.
Stol, W., Rouse, D.I., Kraalingen, D.W.G., Klepper, O., 1992. FSEOPT a FORTRAN Program for Calibration and Uncertainty Analysis of Simulation Models. Simulation Report CABO-TT, No. 24. CABO-DLO and Agricultural University, Wageningen, pp. 24.
ten Berge, H.F.M., Aggarwal, P.K., Kropff, M.J. (Eds.), 1997. Applications of Rice Modelling. Elsevier, The Netherlands, p. 166.
Tsuji, G.Y., Hoogenboom, G., Thornton, P.K., 1998. Understanding Options for Agricultural Production. Kluwer Academic Publishers, The Netherlands, pp. 399–409.
Van den Hoof, C., Hanert, E., Vidale, P.L., 2011. Simulating dynamic crop growth with an adapted land surface model—JULES-SUCROS: model development and validation. Agric. For. Meteorol. 151 (2), 137–153.
Van Laar, H.H., Goudriaan, J., Van Keulen, H., 1997. SUCROS 97: simulation of crop growth for potential and water-limited production situations, as applied to spring wheat. Quantitative Approaches in Systems Analysis, vol. 14. AB-DLO, Wageningen, The Netherlands.
Vazifedoust, M., van Dam, J.C., Bastiaanssen, W., Feddes, R.A., 2009. Assimilation of satellite data into agrohydrological models to improve crop yield forecasts. Int. J. Remote Sens. 30, 2523–2545.
Vogelmann, J.E., Howard, S.M., Yang, L.M., Larson, C.R., Wylie, B.K., Van Driel, N., 2001. Completion of the 1990 National Land Cover Data set for the conterminous United States from Landsat Thematic Mapper data and Ancillary data sources. Photogramm. Eng. Remote Sens. 67, 650–662.
Wolf, J., 2002. Comparison of two potato simulation models under climatic change. I. Model calibration and sensitivity analysis. Climate Res. 21, 173–186.
Xu, W., Jiang, H., Huang, J., 2011. Regional crop yield assessment by combination of a crop growth model and phenology information derived from MODIS. Sens. Lett. 9, 981–989.
Xu, Z., Liu, S., Gong, L., Wang, J., Li, X., 2008. A study on the data processing and quality assessment of the eddy covariance system. Adv. Earth Sci. 23, 357–370.